GSI

GSI-Preprint-98-18
März 1998

STRUCTURE OF HIGH SPIN STATES IN ^{104}Sn - *E*2 AND *E*3 POLARIZATION OF THE ^{100}Sn CORE

M. Gorska, H. Grawe, D. Kast, G. de Angelis, P. G. Bizzeti, B. A. Brown, A. Dewald,C. Fahlander, A. Gadea, A. Jungclaus, K. P. Lieb, K. H. Maier, D. R. Napoli, Q. Pan, R. Peusquens, M. De Poli, M. Rejmund, H. Tiesler

(Submitted to Phys Rev. C)

Gesellschaft für Schwerionenforschung mbH
Planckstraße 1 • D-64291 Darmstadt • Germany
Postfach 11 05 52 • D-64220 Darmstadt • Germany

Structure of high spin states in ^{104}Sn – $E2$ and $E3$ polarization of the ^{100}Sn core

M. Górska[1,2], H. Grawe[1], D. Kast[3], G. de Angelis[4], P. G. Bizzeti[5], B. A. Brown[6], A. Dewald[7], C. Fahlander[4], A. Gadea[4], A. Jungclaus[3], K. P. Lieb[3], K. H. Maier[8], D. R. Napoli[4], Q. Pan[4], R. Peusquens[7], M. De Poli[4], M. Rejmund[1,2], H. Tiesler[7]

[1] *Gesellschaft für Schwerionenforschung, Planckstr. 1, D - 64291 Darmstadt, Germany*

[2] *Institute of Experimental Physics, University of Warsaw, Warsaw, Poland*

[3] *II. Physikalisches Institut, Universität Göttingen, Göttingen, Germany*

[4] *Istituto Nazionale di Fisica Nucleare, Laboratori Nazionali di Legnaro, Legnaro (Padova), Italy*

[5] *Istituto Nazionale di Fisica Nucleare Sezione di Firenze, Firenze, Italy*

[6] *Department of Physiscs and Astronomy and National Superconducting Cyclotron Laboratory, Michigan State University, East Lansing, Michigan*

[7] *Universität zu Köln, Köln, Germany*

[8] *Hahn-Meitner Institute, Berlin, Germany*

(March 13, 1998)

High spin states in ^{104}Sn were identified in the reaction ^{58}Ni(^{50}Cr, $2p2n$) at 200 MeV and 205 MeV beam energies. The γ-ray energies, intensities, multipolarities, and lifetimes of high spin states were measured with the GASP spectrometer array in combination with a plunger apparatus by means of the recoil distance Doppler shift method. The deduced level scheme and transition probabilities are compared to the results of large-scale shell model calculations using three independent two-body interactions. The agreement of the level energies is satisfactory, except for a cascade of dipole transitions at high spins. The general good agreement found for $E2$ transition strengths implies a large effective neutron polarization charge. The shell-model calculations do not account for the measured enhanced $E3$ transitions for which a core excited octupole phonon admixture is indicated.

PACS number(s): 21.10.Tg, 21.60.Cs, 23.20.Lv, 27.60.+j

I. INTRODUCTION

Besides single particle structure and the residual interaction, core excitations of $E2$ and $E3$ type are the most interesting features of a doubly magic nucleus. Until recently little was known in this respect on the $N = Z = 50$ shell closure at ^{100}Sn. With the first results on low lying excited levels and $E2$ transitions in the $T_z = 1$ neighbours ^{98}Cd [1] and ^{102}Sn [2], the $T_z = \frac{3}{2}$ nucleus ^{99}Cd [3] and the $T_z = 2$ nucleus ^{104}Sn [4], controversial evidence on the $E2$ polarization charges for protons and neutrons became available. From the single-particle structure, a large similarity to ^{56}Ni is expected, which due to the LS-open core is subject to strong $E2$ type core excitations [5]. This is corroborated by the systematics of $I^\pi = 2^+$ states, which imply the existence of a low-lying 2^+ state in ^{100}Sn [6]. Also in light Sn isotopes collective bands of magnetic rotation ("shears") character were identified [7], which raises the question, how little deformation is needed to enable this new collective phenomenon. Therefore an experiment was designed to study the high spin structure of ^{104}Sn, which can be reached with reasonable production cross section, and to measure electromagnetic transition rates in this nucleus.

II. EXPERIMENT

The experiment was carried out aiming at the measurement of short lifetimes in the range of several hundred femtoseconds to 0.5 ns in a number of nuclei with $Z \sim 50$ and $N > 50$. The shortest lifetimes, below 1 ps were accessible to the Doppler Shift Attenuation Method (DSAM) [8] with a 0.45 mg/cm^2 thick ^{58}Ni target on a backing made of 50 mg/cm^2 Au. It was not possible to find Doppler broadened lines for ^{104}Sn, but this measurement served to extend the level scheme of this nucleus significantly. For longer lifetimes (1 ps - 0.5 ns) the Recoil Distance Method (RDM) [8] was used with the Cologne plunger [9], and a 1.2 mg/cm^2 thick target of ^{58}Ni and a Au stopper of 12.3 mg/cm^2 thickness. Data were taken for 12 distances ranging from 16 μm to 7 mm, corrected for an offset of 12(3) μm. Each flight distance was set with a piezoelectric linear motor and regulated via a piezo-feedback system, and the capacitance of the target-stopper system.

The experiment was performed at the INFN Laboratory in Legnaro. The ^{50}Cr beam provided by the tandem accelerator had energies of 205 MeV and 200 MeV for the RDM and DSA measurement, respectively. The ^{104}Sn nucleus was populated in the $2p2n$ exit channel from the ^{108}Te compound nucleus with 0.7% of the total population as estimated by the CASCADE computer code [10]. The production cross section extracted in an earlier study of this nucleus was 2mb [4] for the same reaction and a very similar excitation energy of the compound nucleus. There were about 20 other nuclei populated with larger cross section in this reaction.

The γ radiation was measured with the GASP spectrometer [11] with an efficiency increased to ~5% in comparison to the standard value of ~3% by dismounting the BGO inner ball. The distance from the detector to the target was reduced from 24 cm to 17 cm. The beam of ~5 pnA provided by the tandem accelerator and the high efficiency of the GASP allowed for selection of triple γ-ray coincidences as valid events at a rate of $\sim 8 \times 10^3/s$. In addition for the RDM measurement the trigger condition was sharpened by excluding events with three γ rays from a 90 degree ring, consisting of 8 detectors, since they are not subject to a Doppler shift.

The data from the prompt γ-ray experiment were sorted into nonsymmetric energy γ-γ matrices and a symmetrized γ-γ-γ cube. The energy calibration was based on three standard γ-ray sources ^{133}Ba, ^{152}Eu and ^{56}Co for the measured energy range from 70 keV to 3.9 MeV. In the analysis γ-rays were selected from the 50 ns and 200 ns wide prompt windows for double and triple coincidences, respectively. The mutual coincidences and relative intensities of transitions were deduced from the triple matrix and normalized to the 1260 keV ground state transition from the first excited state. The angular distribution intensity ratios of γ-rays were measured at two independent angles ~34°, respectively 145°, and 90° with respect to the beam direction. The nonsymmetric matrices, with γ-ray events from detectors at all angles on one axis and events from detectors at the above given angles only on the other axis, were incremented. The reference values of the intensity ratios were determined from the calculation of angular distributions based on Ref. [12]. The expected ratio values are 0.7 — 0.9 for a stretched dipole, 1.5 — 1.9 for a stretched quadrupole, and ~2.0 for a stretched octupole transition. Since the parities of the states and the multipolarities of the non-stretched transitions cannot be determined from the angular distribution ratios, the assumption of population of predominantly yrast states and decreasing spin with each emitted γ-ray was made. Since the condition of population of yrast states only is not fulfilled in general, most of the spins and parities, that were assigned from the angular distribution intensity ratios, must be considered tentative.

The lifetimes of excited states in the RDM measurement were analyzed from the intensity variation of the stopped component of γ-rays only. The transitions below the long lived 6^+ state ($\tau = 2.2(3)$ ns [4]), where only the stopped component exists, namely 1260, 683 and 314 keV, were used for a gate, selecting ^{104}Sn. Four γ-γ matrices were sorted for each distance. Each matrix was built from γ-rays detected at one of the angles of 34.5°, 145°, 59° , 120.5° in coincidence with any other γ-ray registered. The intensity of the stopped component was normalized for each distance to the total number of counts in the matrix . The high density of γ-ray lines in the γ-γ spectrum made an analysis of the flight component impossible. The correct feeding patterns, as deduced from the γ-ray intensities, were taken into account.

III. RESULTS

The structure of ^{104}Sn was studied for the first time by the Berlin group [4], who assigned seven γ rays at 1260 keV, 683 keV, 314 keV, 1183 keV, 540 keV, 1858 keV and 594 keV to this nucleus and placed them as shown in Fig. 2. The mean lifetime of the $I^\pi = 6^+$ state was determined to $\tau = 2.2(3)$ ns. In the present work the level scheme could be extended up to almost 10 MeV excitation energy, as seen in Fig. 2. The double-gated spectrum shown in Fig. 1 was constructed from the first gate on the 314 keV transition and the second gate on the 1260 keV, 683 keV, 1183 keV or 540 keV lines. There are seventeen γ-rays found in ^{104}Sn and two additional, labeled with stars in Fig. 1, at energies of 250 keV and 612 keV, that could not be placed in the level scheme.

A. Even parity states

The existence of the 6^+ isomer was confirmed in the measurement, with three γ-rays at energies 314 keV, 683

keV, and 1260 keV forming a cascade depopulating this long-lived state, but its lifetime was too long to be measured with the plunger apparatus and could not be remeasured. Their angular distribution ratios clearly indicate a quadrupole character of those transitions (see Table 1). Their order could not be determined since there is no parallel branch observed, and was taken from Ref. [4] and systematics. Similarly two coincident γ rays at energies 1183 keV and 540 keV have quadrupole character. Both transitions show the same lifetime which was well measurable with the plunger method using γ-γ coincidences, yielding $\tau = 150(20)$ ps (see Table 2 and Fig. 3) as the lifetime of the 10^+ state. In addition the weak γ-ray at 1281 keV, feeding the 8^+ state, is not in coincidence with the 540 keV line and therefore determines the order of those two transitions.

B. Odd parity states

The γ-ray flux above the 10^+ state is highly fragmented into many branches. There are three high-energy dipole transitions among them at energies of 1858 keV, 2053 keV and 2104 keV. This high energy of a dipole transition indicates $E1$ character and hence the change of parity of the final state with respect to the initial state. In addition the 1858 keV and 2053 keV dipole transitions form two cascades with the 594 keV and 436 keV transitions, with cross-over transitions at 2452 keV and 2489 keV, respectively (see Fig. 2). The angular distribution intensity ratios indicate quadrupole character for the two lower-energy transitions at 594 keV and 436 keV energy.

For the first triple set of γ-rays, the order of the 1858 keV and 594 keV transitions is firmly determined by a cascade of two transitions (1117 and 1281 keV) feeding the 8^+ state. The quadrupole character of the 594 keV line, and the dipole character of the coincident 1858 keV transition require an octupole cross-over transition. This is supported by the strong anisotropy of the high energy line at 2452 keV, depopulating the same state at 6433 keV energy, and thus assigned to be an octupole transition (see Table 1). ¿From a Weisskopf estimate the competition of a quadrupole 594 keV and octupole 2452 keV transitions is only possible when they are $E2$ and $E3$ transitions, respectively. This determines definitely the 1858 keV transitions to be of $E1$ character. Additionally, the effective lifetime of the state at 6433 keV excitation energy was determined to 63(10) ps based on the information from the 594 keV and 1858 keV lines (see Table 2). This excludes the possibility for the 2452 keV γ ray being an $M3$ transition. Therefore, we propose the 11^-_1 and 13^-_1 assignment for the states at 5839 keV and 6433 keV energy, respectively.

A second weak branch from the 11^-_1 state consists of the 1117 keV and 1281 keV lines. They are both weak and the angular distribution intensity ratios could not be determined. The order of the two γ-rays is based on a very weak coincidence between the 1117 keV and 540 keV transitions, which also explains the significantly higher intensity of the 1117 keV line with respect to the 1281 keV transition. The intermediate level tentatively placed at 4721 keV excitation energy is assigned to have $I^\pi = (9^-)$, based on theoretical arguments (see discussion below). The $(9^-) \rightarrow 10^+$ transition is not observed, which is consistent with its small transition energy. A comparable reduced strength of the two $E1$ transitions would yield less than 20% for the $(9^-) \rightarrow 10^+$ branch, which is below the detection limit of the present experiment.

The second triple set of γ rays at 436 keV and 2489 keV energy, depopulating the state at 6469 keV, and a dipole transition at 2053 keV is very similar to the first one, although experimental information is scarce. The order of the 436 keV line and 2053 keV dipole transition could not be determined from the experiment. Since the 436 keV line is most likely a quadrupole transition, based on angular distribution intensity ratios, the cross-over 2489 keV γ-ray is assigned as the 2452 keV line to an octupole transition (see Table 1). From the systematics of even mass Sn isotopes (see Fig. 4) [2,13,14], even-parity states above the 10^+ in ^{104}Sn are expected at a very high energy, as indicated by the increasing energy of the 14^+ level when going from ^{110}Sn to ^{108}Sn, and the non-observation of any positive-parity state above 5.3 MeV excitation energy in ^{106}Sn, which was studied up to 11 MeV [13]. The energy of the I=11,12,13 negative parity states in this region also increases with decreasing neutron number and is expected to reach 6 MeV in ^{104}Sn. This would confirm a change of parity of the observed states above the 10^+ and would also indicate the order of the 436 keV and 2053 keV γ-rays as shown in Fig. 2. The lifetime of the 6469 keV state could not be measured directly from the 436 keV and 2489 keV lines because excessive background and/or of lack of intensity. The effective lifetime was measured to 52(12) ps, based on the decay curve of the 2053 keV line, which gives an upper limit for the lifetime of the state at 6469 keV. From this limit only the $E3$ possibility is left for this line, which determines the relation of the quadrupole 436 keV and the dipole 2053 keV transitions. There are two possible combinations for these two γ rays: one where the dipole is an $E1$ and the quadrupole is $E2$, and the other $M1$ and $M2$, respectively. The latter possibility is excluded since an $M2$ transition of 436 keV energy would be many orders of magnitude slower than the $\simeq$52 ps limit. Thus an option similar as for the above mentioned three transitions depopulating the (13^-) state is most probable. Therefore the levels at 6032 keV and 6469 keV excitation energy are assigned tentatively to 11^-_2 and 13^-_2 states. The reduced transition strengths for the 436 keV and 2489 keV $E2$ respectively $E3$ transitions appear to be large as compared to the single-particle transition (see Table 2).

The level at 6853 keV excitation energy is depopulated by two dipole transitions at 421 keV and 385 keV energy, which feed the 13^-_1 and 13^-_2 states, respectively. This

is also an argument for identical spin and parity of the two levels at 6469 keV and 6433 keV energy. The lifetime of the state at 6853 keV could not be measured, because of the high density of lines in the 300 - 600 keV energy range, and hence rapidly changing background, but it is likely shorter than the effective lifetimes of the states at 6433 keV and 6469 keV excitation energy. The 421 keV and 385 keV lines are most probably $M1$ transitions, since $E1$ transitions of such low energy are usually not observed. An $E1$ character of these transitions would require a change of parity of the state at 6853 keV energy, with respect to the 13^- states, which again is not expected from the systematics of the Sn isotopes (see Fig. 4). Thus the state at 6853 keV is tentatively assigned to 14^-.

The third high energy dipole transition depopulating the state at 6085 keV is coincident with the 497 keV dipole transition. The cross-over transition is not observed. The very short effective lifetime of 1.0(4) ps deduced from the 2104 keV transition allows $E1$ and $M1$ character of the 2104 keV transition, and $M1$ of 497 keV. The systematics of even Sn isotopes shown in Fig. 4 does not account for any positive-parity yrast state between 4 and 7 MeV, therefore $E1$ multipolarity is assigned to the 2104 keV transition and $I^\pi = 12^-$ to the 6581 keV state. The order of those two transitions could not be determined from the intensity balance (see Table 1) and is based on theoretical arguments. The proposed order indicates spin $11\hbar$ and tentative negative parity of the state at 6085 keV. The level at 7125 keV excitation energy, depopulated by the 544 keV dipole and most probably $M1$ transition, is tentatively assigned to the 13^-_3 state.

C. States above $E_x = 8$ MeV

For the state at 7997 keV excitation energy and higher lying states no spin assignments were possible because of lack of experimental information for the connecting transitions. On the basis of the measured γ-ray anisotropies, the cascade on top of this state has dipole character. Due to statistical uncertainties the order of these γ-rays remains undetermined. From the dipole character of these transitions, and the fact that no further shell-model states are expected at this energy, we suuggest that these states represent proton particle-hole excitations. In the neighbouring nucleus ^{105}Sn a similar band structure has been identified as a magnetic rotation shears band [7].

IV. DISCUSSION

The interpretation of the level scheme shown in Fig. 2 is based on the coupling of four valence-neutron particles in ^{104}Sn, that occupy in the ground state the $(d_{5/2},g_{7/2})^4$ configuration outside the closed ^{100}Sn core. There are indications [15] that these two orbitals are almost degenerate.Two neutrons scattered within those two orbitals give to the nucleus a maximum spin of $6\hbar$, which is the maximum spin for this multiplet in ^{102}Sn and is indicated with a black dot in Fig. 4. The $E2$ type of the transitions connecting those states indicates two-quasiparticle character up to the 6^+ state, similarly as recently found for ^{102}Sn [2]. The breaking of a second pair of neutrons is indicated by the characteristic increased energy of the 1183 keV $8^+ \rightarrow 6^+$ transition. The observation of a energy gap between 3981 keV and 5839 keV indicates raising one neutron to the $h_{11/2}$ orbital and hence a change of parity of the levels above the 10^+ state. The exception is made for a state at (4721 keV) energy, that is fed only by a weak γ-ray of 1117 keV. It is assigned to a $I^\pi = (9^-)$ two-quasiparticle state that results likely from the coupling of the configuration $(d_{5/2},g_{7/2})^2_{0^+}$ for one pair of neutrons and $g_{7/2}h_{11/2}$ for the other pair of valence neutrons. It is also in agreement with the energy of the 9^- state expected from the systematics of Sn isotopes (Fig. 4). From one particle in the $h_{11/2}$ shell and three in the $d_{5/2}$, $g_{7/2}$ orbitals the maximum spin of $14\hbar$ is expected in the energy region of other negative parity states, which is confirmed by the systematics. More than one configuration for $I^\pi = 11^-$ and 13^- is expected, which also is supported by the experimental observation. The state at 6085 keV is assigned to a 11^-_3 state based on the argument of a high lying $h_{11/2}$ shell and no other possibility of gaining spin above the 10^+ state as found for the 11^-_1 and 11^-_2 states. Still higher-spin levels observed in the experiment have to be explained by raising a second neutron to the $h_{11/2}$ orbital. This costs additional $\simeq 2$ MeV in excitation energy. The observed gap in the experiment between 6853 keV and 7997 keV, on which a cascade of dipole transitions is built, seems to be significantly lower. In this energy region also core excitations of protons and neutrons are expected [7]. The cascade of dipole transitions is most probably built on core excitations, and may be related to the magnetic rotation found recently in ^{105}Sn [7], where a regular band of dipole transitions is observed. The expected transitions are of $M1$ type. The phenomena of magnetic rotation have been explained by Frauendorf [16] as closing together the angular momentum vector of a few aligned, high-j proton holes towards that of a few, initially strongly coupled, high-j neutrons, which at the bandhead are almost at right angle. For the nuclei in the ^{100}Sn region the configuration suited for this structure is $\pi(g^{-1}_{9/2}g_{7/2})$ coupled to neutrons in the $h_{11/2}$ orbit and in the orbits originating from the mixed $d_{5/2}$ and $g_{7/2}$ multiplets [7].

A. Shell model calculation and level scheme

We have performed calculations using the shell-model code OXBASH [17] for three independent sets of two-body matrix elements in the $\nu 2d_{5/2}, 1g_{7/2}, 3s_{1/2}, 2d_{3/2}$

and $1h_{11/2}$ model space. The results of the calculations are shown in Fig. 2 for each type of interaction. The first set of neutron-neutron interactions named EMP was obtained from a realistic interaction in combination with scaled matrix elements from the lead region for multiplets involving the $1h_{11/2}$ orbital. For details of the interaction see Ref. [4,18]. The second set of interaction BR was obtained from scaled matrix elements for $N = 82$ nuclei [19]. The third type of realistic effective interactions REI is obtained from Ref. [20]. They are based on a perturbative many-body description with the most recent meson-exchange potential models for the nucleon-nucleon interaction. The adopted single-particle energies are shown in Table 3. Since the low spin $d_{3/2}$ and $s_{1/2}$ orbital energies are not well determined, as they are not observed in the yrast states populated in the fusion-evaporation reactions, they might be varied within a range of ~ 1 MeV. The model space was restricted only for the case of the EMP interaction to the maximum of three particles dsitributed in the $d_{3/2}$, $s_{1/2}$ and $h_{11/2}$ orbitals.

The shell model space involving the lowest lying $\nu 2d_{5/2}, 1g_{7/2}$ orbitals is exhausted with $I^\pi = 10^+$ for ^{104}Sn , while the spin 12^+ is still possible in ^{106}Sn (see Fig.4). The states up to 10^+ are rather well reproduced in all three calculations. The significantly lower energy of the $3s_{1/2}$ orbital in the REI calculations causes a larger splitting of the 4^+ and 6^+ levels, which is closer to the experimental value than the two other calculations. The excitation of one neutron into the $1h_{11/2}$ orbital is indicated by changing the parity of the states to negative up to spin $14\hbar$, while two neutrons in the $1h_{11/2}$ orbital change the parity to positive again for the 15^+ and 16^+ states. All the experimental levels in the range of excitation energy 5.8 - 7.2 MeV could be accounted for in the calculations as seen in Fig. 2. The three different sets of interactions show small deviations in level energies. ^{104}Sn is the highest $Z = 50$ isotope where the energy spacing between the $\nu 2d_{5/2}$ and the $\nu 1h_{11/2}$ orbitals may be explicitly visible by observation of the $E3$ transition $(2d_{5/2}, 1g_{7/2})^3 h_{11/2}:13^- \rightarrow (2d_{5/2}, 1g_{7/2})^4:10^+$. While the $11_1^- \rightarrow 10^+$ transition energy is well reproduced in all calculations the energy of the 13_1^- state is significantly reduced in the BR and REI calculations. The 11_2^- and 11_3^- energies are reproduced best with the BR interaction, while in the EMP and REI calculations do not agree as well with the experiment. This might be related to the small single particle energy difference between the $1g_{7/2}$ and $2d_{5/2}$ orbitals for the BR calculations. In all three calculations the energy between the 13_2^- and 13_1^- states could not be reproduced, while the agreement is good for the 13_3^- and 13_1^- splitting energy and the $12^-, 14^-$, and 13_3^- states. In the BR single-particle energies, a shift of $\simeq 100$ keV of the $1h_{11/2}$ energy should be considered. The energies of the dipole band found in the experiment above 7.9 MeV excitation energy can not be reproduced in any of the calculations, and thus are considered to originate from outside the model space. This would be a confirmation of the origin of these states from core excitations.

B. Electromagnetic transition strengths

The comparison of the experimental reduced transition probabilities with the calculations is shown in Table 2. The $E2$ transition strength from the two-quasiparticle 6^+ state, known from a previous measurement [4], is not reproduced by any calculation if the usual neutron effective charge of 1.44 is used [4], as throughout this paper. The main component of the $6^+ \rightarrow 4^+$ transition in the calculation is the so called spin flip $1g_{7/2}2d_{5/2}^3 \rightarrow 1g_{7/2}^2 1d_{5/2}^2$, which has a small reduced matrix element, and thus produces a small B(E2) value. A significant improvement is achieved when the single particle energy of the $3s_{1/2}$ orbital is reduced, i.e. its binding energy is increased. The wave function of the 4^+ state then contains more of the $1g_{7/2}3s_{1/2}$ configuration, which is not possible for the 6^+ state, and hence the total reduced matrix element is increased by a strong stretched component $1g_{7/2}2d_{5/2} \rightarrow 1g_{7/2}3s_{1/2}$. A similar behavior is observed for the $10^+ \rightarrow 8^+$ reduced transition probability. For the BR calculations this value is too large which is caused most probably by the different single-particle energies of the $1g_{7/2}$ and $2d_{5/2}$ orbitals with respect to the other calculations. This corroborates the large effective neutron charge used in the present work and excludes even larger values as has been invoked earlier [4]. Recently the $6^+ \rightarrow 4^+$ transition in ^{102}Sn was studied yielding a similar effective charge [21]. The sensitivity of the B(E2) values to the single-particle energies, which presently are not known precisely [18], should be taken as a sign of caution in the discussion of the effective neutron charge. The large effective charge is pointing to a low-lying $I^\pi = 2^+$ state in ^{100}Sn as also deduced from the systematics of $I^\pi = 2^+$ energies in ^{56}Ni and ^{100}Sn isotopes and isotones [6]. This is at variance with the small polarization charge found for protons in ^{98}Cd [1].

Reasonable agreement of the calculation with experiment is found for the $12^- \rightarrow 11^-$ $M1$ transition when the calculated 11_2^- state is taken instead of the 11_3^-. This change was also applied to the $13_2^- \rightarrow 11^-$ $E2$ transition, did however not improve the discrepancy with experiment. In general the $13^- \rightarrow 10^+$ $E3$ transition strengths are not reproduced by the calculations when an effective $E3$ neutron charge of 1.0 is used. They are the first octupole transitions found in light Sn isotopes. Especially the $E3$ decay of the 13_2^- state is very strong and cannot be interpreted as a single-particle transition. The lower limit of $B(E3) \geq 17$ W.u. indicates an admixture of the collective phonon vibration of the ^{100}Sn core to the stretched single particle $1h_{11/2} \rightarrow 2d_{5/2}$ transition as known in the ^{208}Pb [22,23] and ^{132}Sn [24] double magic regions for appropriate single particle orbitals. There the strong $E3$ transition is observed directly in the core

nuclei. The present experiments therefore establish the first indication of an $E3$ core excitation in the ^{100}Sn region. The prediction of the 3^- phonon energy and its strength is difficult because of the treatment of particle-hole excitations. In general it is expected to have at least $\hbar\omega_3 = 4$ MeV, and a $B(E3)$ strength of $\simeq 30$ W.u.. Thus one expects a large admixture of the octupole phonon in the $13_2^- \rightarrow 10^+$ transition, which would further indicate comparable energies of the phonon and the 2489 keV γ-ray. The coherent interaction of protons and neutrons in identical orbitals in ^{100}Sn may cause an effective decrease of the phonon energy and a stronger coupling to the shell model states. The microscopic structure of the 3^- particle-hole excitation in ^{100}Sn may consists of two dominating $2p_{1/2}^{-1}1g_{7/2}$ and $2p_{1/2}^{-1}2d_{5/2}$ configurations, which build the strong matrix element for the transition because of their stretched coupling of single particle orbital angular momenta. To confirm this phenomenon in the ^{100}Sn region the knowledge of the high spin states in the closer neighbours of the core nucleus is indispensable.

V. CONCLUSION

High spin states in ^{104}Sn up to 10 MeV excitation energy were studied in $\gamma\gamma\gamma$ coincidences, and $E2$ and $E3$ transition strengths were determined from recoil distance lifetime measurements. Indications for a high lying magnetic dipole band with shears character is found. For the first time in the ^{100}Sn region enhanced $E3$ transitions were identified, which imply a low-lying (~ 3 MeV) $I^\pi = 3^-$ octupole phonon in ^{100}Sn. For $E2$ transitions a large effective neutron charge was found, which along with the systematics of 2^+ states in ^{56}Ni and ^{100}Sn isotones and isotopes, points to a low lying (≤ 3 MeV) $I^\pi = 2^+$ state in ^{100}Sn. This is the first step for a systematic investigation of core excitations in ^{100}Sn, which opens the field for high precision studies with the new γ arrays EUROBALL and Gammasphere.

ACKNOWLEDGMENTS

The authors appreciate the excellent cooperation of the staff of the INFN laboratory in Legnaro. We are grateful to Profs. J. Blomqvist, E. Osnes and J. Wood for valuable discussions.

[1] M. Górska, et al., *Phys. Rev. Lett.* **79** (1997) 2415.
[2] M. Lipoglavšek, et al., *Z. Phys.* **A356** (1996) 239.
[3] M. Lipoglavšek, et al., *Phys. Rev. Lett.* **76** (1996) 888.
[4] R. Schubart, H. Grawe, J. Heese, H. Kluge, K. H. Maier, M. Schramm, *Z. Phys.* **A352** (1995) 373.
[5] G. Kraus, et al., *Phys. Rev. Lett.* **73** (1994) 1773.
[6] H. Grawe, et al., *Z. Phys.* **A358** (1997) 185.
[7] A. Gadea, et al., *Phys. Rev.* **C55** (1997) R1.
[8] P. J. Nolan, J. F. Sharpey-Schafer, *Rep. Prog. Phys.* **42** (1979) 1.
[9] A. Dewald et al., *Nucl. Phys* **A545** (1992) 822.
[10] F. Pühlhofer, *Nucl. Phys.* **A280** (1977) 267.
[11] GASP Collaboration Report, INFN/BE-90/11 (1990), C. Rossi-Alvarez, *Nucl. Phys. News Europe* **3 (3)** (1993) 10.
[12] T. Yamazaki, *Nucl. Data.* **A3** (1967) 1.
[13] S. Juutinen, et al., *Nucl. Phys.* **A617** (1997) 74.
[14] R. B. Firestone, V. S. Shirley, Table of Isotopes **I**, Eighth Edition, A Wiley-Interscience Publication, 1996.
[15] H. Grawe, R. Schubart, D. Alber, R. Alfier, D. B. Fossan, J. Heese, H. Kluge, K. H. Maier, M. Schramm, *Prog. Part. Nucl. Phys.* **28** (1992) 281.
[16] S. Frauendorf, *Nucl. Phys.* **A557** (1993) 259c.
[17] B. A. Brown, A. Etchegoyen, W. D. M. Rae, code OXBASH (1984) unpublished.
[18] H. Grawe, R. Schubart, K. H. Maier, D. Seweryniak, *Phys. Scr.* **T56** (1995) 71.
[19] B. A. Brown, K. Rykaczewski, *Phys. Rev.* **C50** (1994) R2270.
[20] M. Hjorth-Jensen, T. T. S. Kuo, E. Osnes, *Phys. Rep.* **261**(3 & 4) (1995) 125.
[21] M. Lipoglavšek, et al., to be published.
[22] Aa. Bohr, B. Mottelson, *Nuclear Structure* vol. II. Benjamin, London, (1975) p.416 and 564.
[23] M. Rejmund et al., to be published.
[24] J. P. Omtvedt, M. Mach, B. Fogelberg, D. Jerrestam, M. Hellström, L. Spanier, K. I. Erokhina, V.I. Isakov, *Phys. Rev. Lett.* **75** (1995) 3090.

TABLE I. Energies, intensities and angular distribution intensity ratios $(I(34°)+I(146°)/I(90°)$ for the γ rays belonging to ^{104}Sn.

E_γ [keV]	I_γ	Intensity Ratios	$I_i^\pi \rightarrow I_f^\pi$
314.2(1)	94(2)	1.89(8)	$6^+ \rightarrow 4^+$
384.6(2)	7(1)	0.8(3)	$(14^-) \rightarrow (13_2^-)$
411.7(3)	8(2)	0.8(3)	
421.1(2)	28(2)	0.8(2)	$(14^-) \rightarrow (13_1^-)$
436.1(2)	13(2)	1.5(4)	$(13_2^-) \rightarrow (11_2^-)$
445.9(2)	16(2)	0.8(2)	
496.5(2)	19(2)	0.8(2)	$(12^-) \rightarrow (11_3^-)$
540.2(1)	81(3)	1.81(9)	$10^+ \rightarrow 8^+$
544.1(3)	8(1)	0.9(2)	$(13_3^-) \rightarrow (12^-)$
547.1(3)	16(2)	1.0(3)	
594.0(1)	33(3)	1.4(2)	$(13_1^-) \rightarrow (11_1^-)$
597.2(3)	14(2)	1.2(3)	
682.8(1)	93(2)	1.68(8)	$4^+ \rightarrow 2^+$
1117.0(5)	11(2)		$(11_1^-) \rightarrow (9^-)$
1143.5(4)	13(2)		$\rightarrow (14^-)$
1183.1(1)	97(2)	1.81(9)	$8^+ \rightarrow 6^+$
1260.2(1)	100(2)	1.60(9)	$2^+ \rightarrow 0^+$
1281.1(5)	7(2)		$(9^-) \rightarrow 8^+$
1564.8(5)	4(2)		$\rightarrow (13_1^-)$
1858.5(3)	26(3)	0.9(2)	$(11_1^-) \rightarrow 10^+$
2053.2(4)	11(2)	0.8(3)	$(11_2^-) \rightarrow 10^+$
2104.0(4)	19(2)	0.9(2)	$(11_3^-) \rightarrow 10^+$
2451.8(5)	6(2)	2.0(3)	$(13_1^-) \rightarrow 10^+$
2488.7(5)	6(1)	2.1(3)	$(13_2^-) \rightarrow 10^+$

TABLE III. Single particle energies used in three different shell model approaches.

Orbital $n\,l\,j$	EMP	BR Energy [MeV]	REI
$2d_{5/2}$	-11.13	-10.15	-11.13
$1g_{7/2}$	-10.93	-10.10	-10.93
$3s_{1/2}$	-9.30	-8.40	-10.23
$2d_{3/2}$	-9.20	-8.09	-9.63
$1h_{11/2}$	-8.60	-7.85	-8.43

TABLE II. Extracted lifetimes and transition probabilities B($\sigma\lambda$) for ^{104}Sn in comparison to calculations. The lifetimes measured indirectly are indicated by a superscript.

E_x [keV]	I_i^π	τ [ps]	I_f^π	E_γ [keV]	$\sigma\lambda$	B_{EXP} [W.u.]	B_{EMP} [W.u.]	B_{BR} [W.u.]	B_{REI} [W.u.]
2257	6^+	2200(300)[a]	4^+	314	E2	4.1[a]	0.76	2.5	2.15
3440	8^+	< 20	6^+	1183	$E2$	> 0.6			
3981	10^+	150(20)	8^+	540	$E2$	4.1(6)	1.82	8.7	3.32
5839	(11_1^-)	< 8	10^+	1858	$E1$	$> 6 \times 10^{-6}$			
5839	(11_1^-)	< 8[b]	(9^-)	1117	$E2$	> 0.6[b]	6.3	2.7	8.15
6085	(11_3^-)	1.0(4)	10^+	2104	$E1$	$\geq 3.4 \times 10^{-5}$			
6433	(13_1^-)	63(10)	(11_1^-)	594	$E2$	≥ 4.2	7.3	2.3	9.2
6433	(13_1^-)	63(10)[d]	10^+	2452	$E3$	≥ 7[d]	0.01	6.3	0.03
6469	(13_2^-)	52(12)[e]	(11_2^-)	436	$E2$	≥ 17[e]	1.3	0.1	5.7
6469	(13_2^-)	52(12)[e]	10^+	2489	$E3$	≥ 17[e]	7.3	0.5	1.9
6581	(12^-)	≤ 1.4[c]	(11_3^-)	497	$M1$	≥ 0.17[c]	4×10^{-4}	0.004	0.007
	(12_1^-)		(11_2^-)				0.12	0.012	0.08

[a] value known from previous measurement [4]
[b] value deduced from RDM analysis of the 1.858 MeV transition
[c] value deduced from RDM analysis of the 2.104 MeV transition
[d] value deduced from RDM analysis of the 0.594 MeV transition
[e] value deduced from RDM analysis of the 2.053 MeV transition

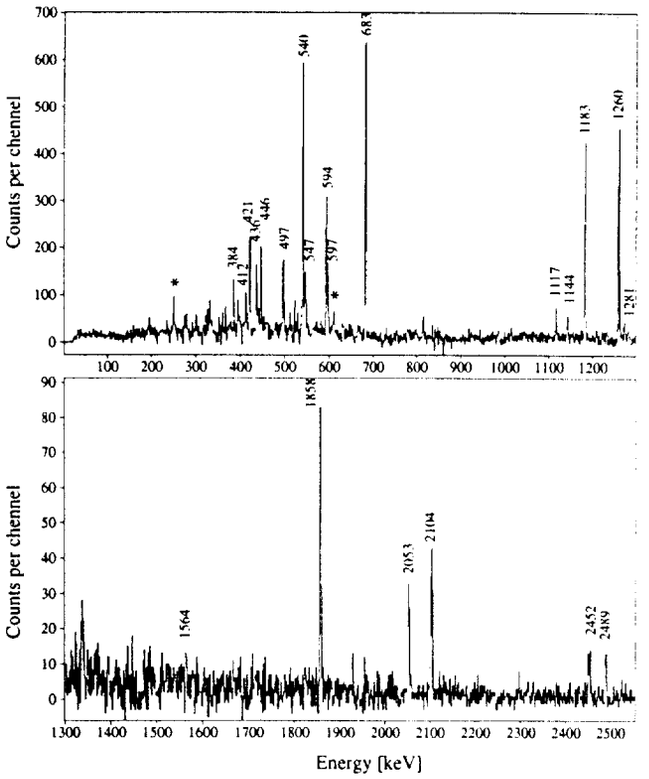

FIG. 1. The triple γ-γ-γ coincidence spectrum obtained from a gate on the 314 keV line in the sum of four γ-γ matrices gated with the 1260 keV, 682 keV, 1183 keV, 540 keV lines in ^{104}Sn.

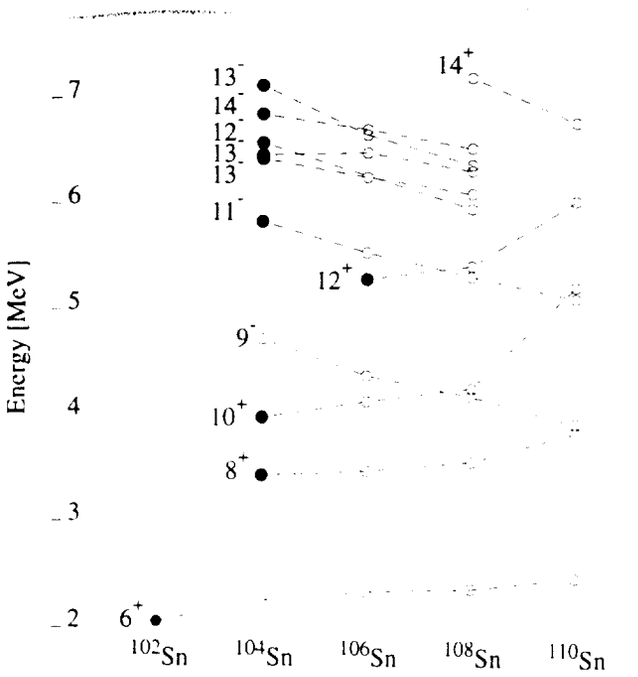

FIG. 4. Systematics of selected yrast and yrare states in even mass Sn isotopes. The spins of the levels are indicated next to the corresponding lines. Black dots indicate the last nucleus where a given spin-parity multiplet is possible to be formed.

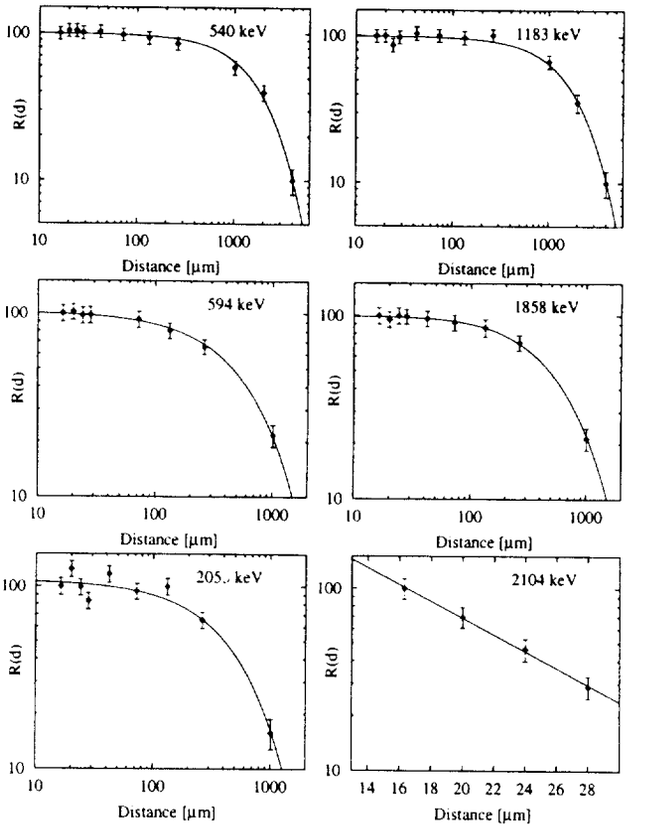

FIG. 3. Normalized intensity of the stopped component of a given γ-ray as a function of the distance between target and stopper. The lines show the best fit obtained after taking into account the feeding pattern.

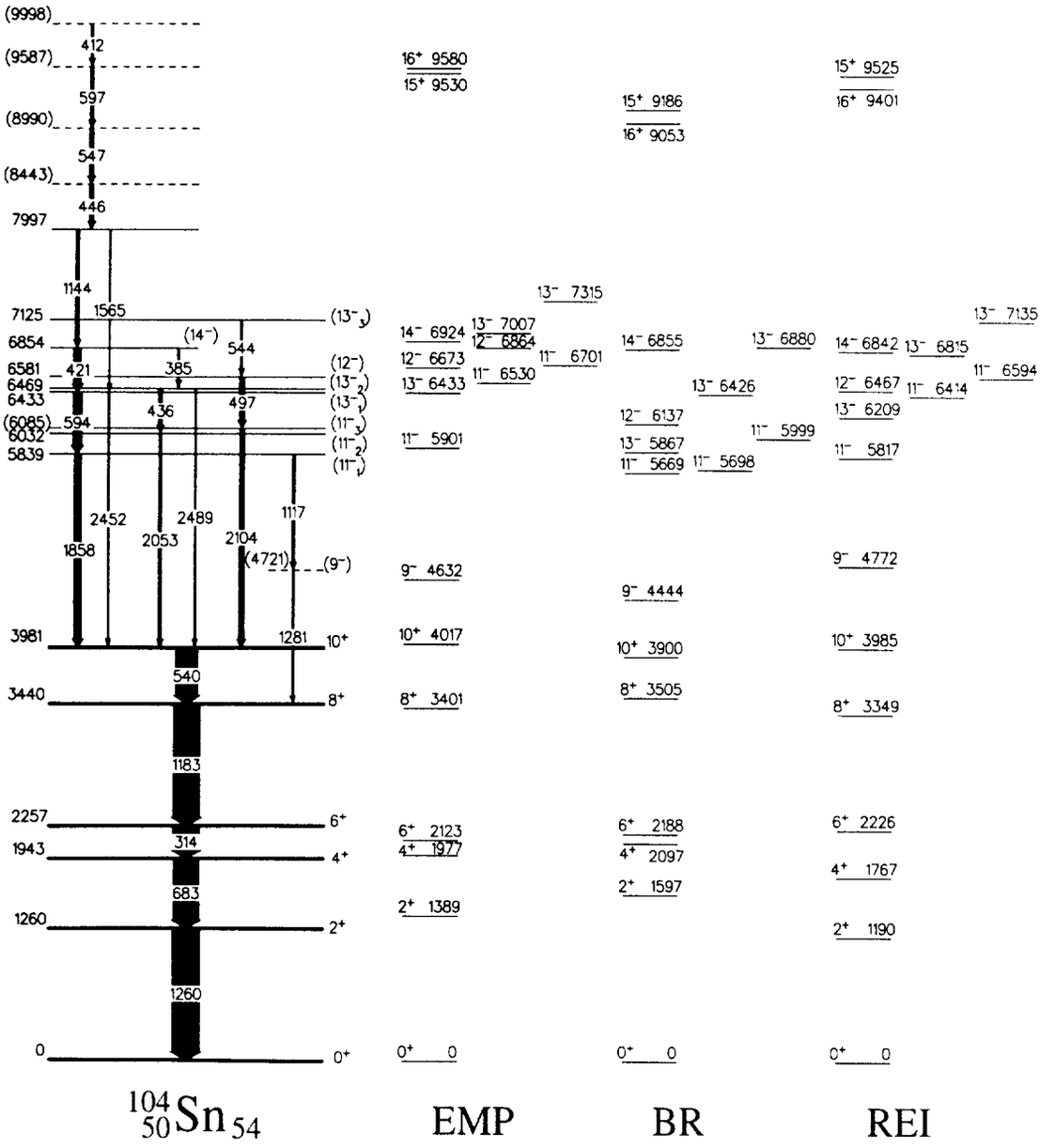

FIG. 2. The level scheme adopted for ^{104}Sn based on mutual γ-γ-γ coincidences, extracted information on γ-ray multiplicities and lifetimes of excited states. On the right hand side the shell model approach of three independent calculations is shown for comparison.